03

Temperature of a laser-induced cavitation jet generated at the tip of an optical fiber immersed in a liquid

© E.P. Dats, A.V. Kulik, M.A. Guzev, V.M. Chudnovskii

Institute for Applied Mathematics, Far East Branch, Russian Academy of Sciences,
690041 Vladivostok, Russia
e-mail: datsep@gmail.com

Received August 8, 2025
Revised November 25, 2025
Accepted November 26, 2025

The temperature of a cavitation jet generated by laser cavitation at the end of an optical fiber immersed in water was studied experimentally and numerically. Laser heating and boiling of subcooled water are caused by continuous laser radiation with a wavelength of $\lambda = 1.47\,\mu$m propagating along the optical fiber (thermal cavitation). It was shown that less than 4% of the volume of the superheated liquid transforms into the vapor phase. The remaining superheated water, distributed over the surface of the vapor bubble, cools during its growth and collapse, and then transforms into a cavitation jet. The jet temperature during a single bubble growth and collapse event reaches 60 °C, which can be used in medical and technical applications.

Keywords: cavitation jet, optical fiber, laser radiation.

DOI: 10.61011/TP.2026.04.63258.207-25

Introduction

The temperature of a cumulative jet originating during asymmetric collapse of the cavitation bubble is a fundamental parameter that is practically important in technical applications and medicine. This parameter is especially important when cavitation occurs during heating and boiling-up of a subcooled liquid [1–14]. Subcooling boiling occurs during local boiling-up of a certain selected liquid volume surrounded by a „cold“ medium, whose temperature is below the saturation temperature. The bubble originating at this, first grows and then, due to a contact with „cold“ environment, acceleratedly collapses when reaching a maximum size, which properly identifies it as a cavitation one [2,4,5]. During laser heating of the liquid subcooling boiling can be initiated both by means of pulsed (laser cavitation) [3,4,7–9] as well as continuous (thermocavitation) [2,5,6,10–14] laser radiation. Mechanisms of heating and boiling-up of the liquid when using pulsed and continuous laser radiation can significantly differ, thereby affecting characteristics of the cumulative jet, but determination of the temperature of this jet is still unsolved.

In the present study, we have investigated cavitation initiated by laser heating of water around an end face of the optical fiber, along which continuous laser radiation propagates [2,5,6,14]. It is very convenient to use the optical fiber, since it is highly flexible and can penetrate narrow channels, tubes, slits and needles for percutaneous impact, thereby making it possible to generate cavitation bubbles in conditions, when it is difficult or impossible to use other methods.

Formation of the cavitation jets during boiling-up of the subcooled liquid around the end face of the quartz optical fiber (cylinder) is described in the studies [2,5], which demonstrate that collapse of a vapor bubble results in two cumulative jets — one is directed towards the end face, so is the other from the end face deep into the liquid. The present study used methods of computational modeling to estimate the temperature of the jet that results from collapse of the vapor bubble and propagates along the direction from the end face of the optical fiber. Parameters of a mathematical model, which are related to a mass exchange process are selected based on experimental data obtained. Special attention is paid to calculating an initial temperature field of water at the moment of appearance of the vapor bubble.

1. Experimental method of the studies and the measurement results

A series of experiments was taken to determine an average time of water heating at the specified parameters of laser radiation from a start of laser operation to appearance of the cavitation bubble. It also included determination of the maximum size of the bubble, the average time of growth and collapse of the vapor bubble as well as the time of formation of the cumulative jet. The experimental data were used for validating the mathematical model of vapor formation-condensation.

Heating and boiling-up of water under effect of continuous laser radiation of the wavelength $\lambda = 1.47\,\mu$m were studied in the experiment using the high-speed videocamera Photron Fastcam SA-Z. Two methods were used for shooting: under direct illumination and in the shadowgraph mode. The first method provides clear fixation of a structure of the vapor phase, whereas the second method makes

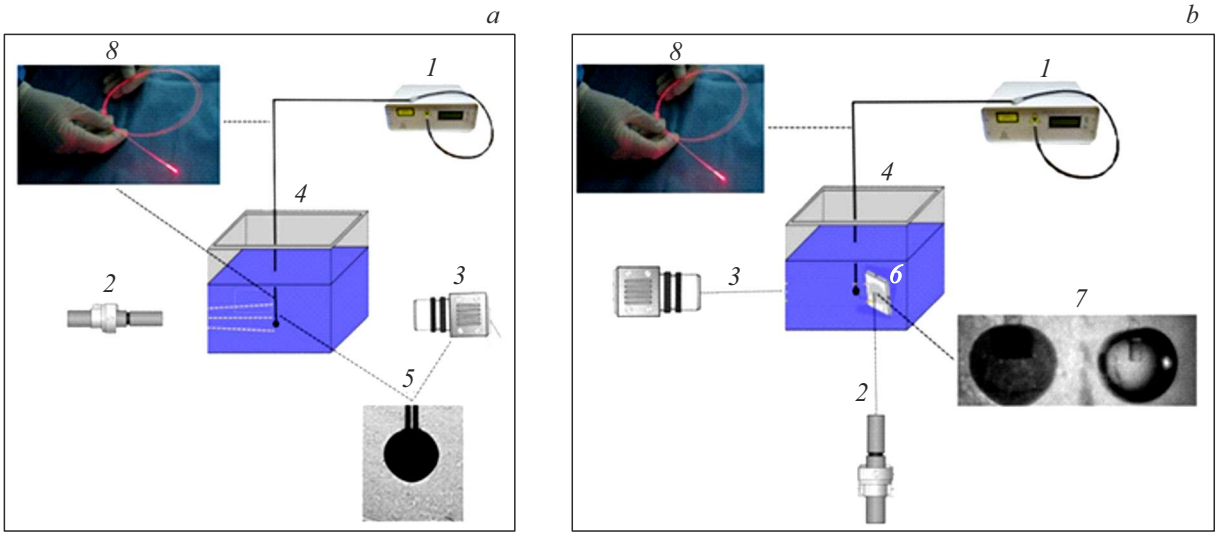

Figure 1. Diagram of the experimental unit for recording an elementary event of boiling-up of subcooled water around the tip of the optical fiber: *a* — the shadowgraph mode, *b* — the direct illumination mode. *1* — laser with the radiation wavelength $\lambda = 1.47\,\mu$m; *2* — the illuminating laser with the radiation wavelength of $\lambda = 0.52\,\mu$m; *3* — the high-speed video-camera; *4* — the working cuvette with water; *5* — the „at lumen“ image of the bubble; *6* — the light-reflecting screen; *7* — the image of the bubble and its shadow on the screen under direct illumination; *8* — the optical fiber.

it possible to well trace dynamics of a region of heated liquid, which is due to variation of a liquid's refractive index that depends on the temperature [15]. The obtained images were in the digital format processed pixel by pixel in order to determine coordinates of an interphase boundary of the bubble. A pixel size is $(35 \pm 15)\,\mu$m. In the experiment, laser radiation propagates along the optical fiber, whose quartz end with the diameter of $600\,\mu$m is submersed vertically downwards in distilled undeaerated water. Water is in the cuvette with the sizes $125 \times 23 \times 41$ mm at the temperature $T = 16\,^{\circ}$C.

Fig. 1, *a* shows a diagram of the experimental unit designed to observe dynamics of heating and boiling-up of the liquid near the end of the optical fiber in the shadowgraph mode. In the experiment, illuminating laser radiation with the wavelength $\lambda = 0.52\,\mu$m illuminates the cuvette along the line that connects a video-camera lens and an illuminating source. At the same time, the video-camera lens catches a shadow of the end of the optical fiber, along which laser „working“ radiation with the wavelength $\lambda = 1.47\,\mu$m propagates, and the liquid surrounding the end of the optical fiber. When exiting the end face of the optical fiber, working radiation is absorbed in water with the coefficient $k \sim 2850\,\text{m}^{-1}$ [16], thereby resulting in effective heating and subsequent local boiling-up of subcooled water around the end of the optical fiber.

Fig. 2 shows a „shadow“ graph of heating and boiling-up of subcooled water around the end face of the optical fiber, which is obtained according to the diagram of the Fig. 1, *a*. When heating, the water density decreases, thereby resulting in deviation of illuminating radiation rays and the shadow of the heated area of water is clearly recorded in the video-camera lens. The water heating area is shown in frames *1*–*7* (Fig. 2), where an enlarging darkened area originates under the end face of the optical fiber as the liquid is heated. The time of water heating is a relatively long period of 70 ms. Then water boils up to form the vapor bubble that enlarges and collapses for 0.46 ms, which is approximately in 150 times less than the time of water heating. The shadowgraph of subcooling boiling-up, in which the bubble first grows and then collapses, is shown in the frames *8*–*12* in Fig. 2. At the moment of maximum collapse (the frame *12* in Fig. 2) a „needle“ jet starts forming [9], which almost immediately results in secondary boiling-up in the moving liquid (a rebound) [14] (the frame *13* in Fig. 2). A submerged jet is determined after collapse of the secondary bubble in the frame *14* in Fig. 2.

In the method of shadow video recording the start of the boiling-up process (intense vapor formation) is determined by a sharp increase of the shadow area (in more than 100 times) (the frames *8*–*10* in Fig. 2). But this method does not make it possible to directly observe the vapor bubble separately from the area of the heated liquid. The moment of appearance of the vapor bubble shall be defined exactly, which is clearly registered in the „direct illumination“ method, when the video-camera lens catches scattered radiation from the area where the liquid boils up. Therefore, in order to register the vapor bubble and same-moment registration of its shadow a configuration of the experimental unit and the experimental diagram were changed. In order to register the vapor bubble against a backdrop of its shadow, the cuvette with water was provided with a flat light-reflection screen behind the optical fiber, which was an opaque aluminum plate installed at the angle of 45° to the axis connecting the tip of the optical fiber and the video-camera lens (Fig. 1, *b*). At the same time,

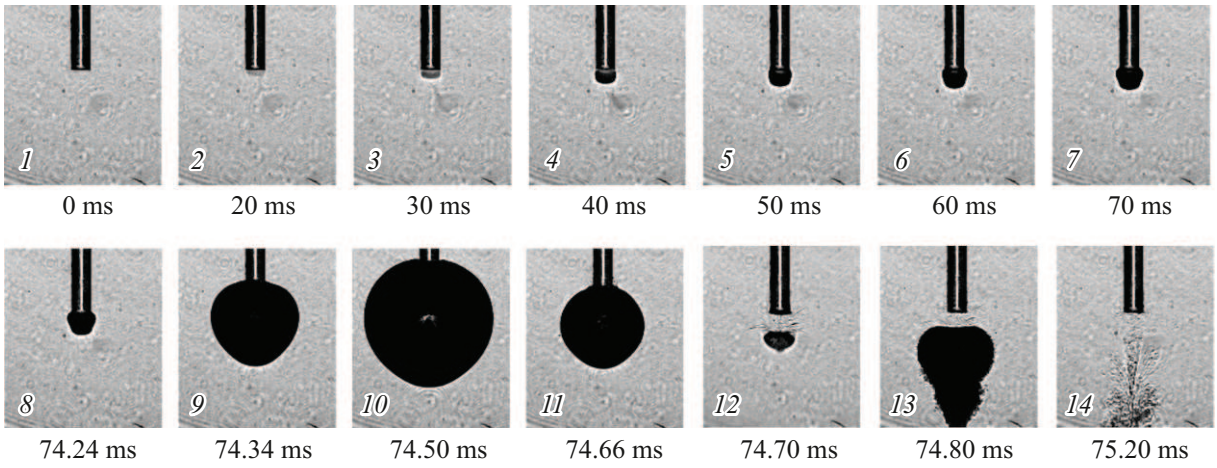

Figure 2. Elementary event of water boiling-up around the end of the optical fiber. A recording rate is 252 000 fps.

the illuminated source was turned by 900 to the camera so that it created the shadow image on the screen, while at the same moment with the shadow image an image of the optical fiber and the bubble appeared in reflected light.

To the right of the dashed line the frames in Fig. 3 show the image of the end of the optical fiber and the bubble in reflected light (direct illumination) and their shadow to the left. The bubble appears on the surface of the end face of the optical fiber to the right in the frame *3* in Fig. 4 and then enlarges with capture of the end of the optical fiber immersed in water. The shadow of this process is at the same moment registered to the left. The frame *1* in Fig. 3 corresponds to the moment of start of operation that warms up water of the laser unit ($t = 0$ ms). To the left in the frame *2* (Fig. 3) that corresponds to the moment of time $t = 68.47$ ms, there is a shown shadow cast by the end of the optical fiber and the area of warmed-up water under the end face of the optical fiber. The frame 3 (Fig. 3) includes a moment of appearance of the vapor bubble on the end face of the optical fiber (the right part of the frame *4* (Fig. 3)). The frames *3*–*6* (Fig. 3) demonstrate growth of the vapor bubble and its shadow. The frame *6* corresponds to the maximum size of the bubble. Then the bubble starts collapsing (the frames *7*, *8*). In this experiment, the time of water heating (the frames *1*, *2* in Fig. 3) approximately in 170 times exceeds the time of growth of the bubble from the moment of its appearance to achieving the maximum size.

An average growth rate of the bubble between the frames *4*, *5* in Fig. 3: $V \approx 9.1$ m/s, and between the frames *5*, *6*: $V \approx 2.2$ m/s.

Fig. 4 marks out the moment of appearance of the vapor bubble. The frame *1* (Fig. 4) has no bubble, whereas the next video frame exhibits the bubble with the diameter of $(50 \pm 15)\,\mu$m in $5\,\mu$s. After another $5\,\mu$s the bubble reaches $(250 \pm 15)\,\mu$m in its diameter. Hence, the average growth rate of the bubble between the frames *2*, *3* is 20 m/s.

As it enlarges, the bubble „pushes apart“ the surrounding heated liquid that forms a heated layer on the surface of the growing and collapsing bubble.

By knowing the volume of the liquid heated to the moment of boiling-up and comparing it with the volume of the vapor phase at the moment when the bubble reaches the maximum size, it is easy to obtain a mass fraction of boiled-up water from preheated one. A ratio of weights of boiled-up water: m_2 (the weight of vapor that fills the bubble when it reaches the maximum size) to the weight of heated water: m_1:

$$m_2/m_1 = \rho_2 V_2/\rho_1 V_1 = \frac{\rho_2}{\rho_1}\left(\frac{D_2}{D_1}\right)^3,$$

where $\rho_2 \approx 0.6\,\text{kg/m}^3$ is a vapor density at the temperature of 100 °C; V_2 is a maximum value of the vapor bubble with taking into account subtraction of the volume of the optical fiber's end immersed in the bubble; $\rho_1 \approx 10^3\,\text{kg/m}^3$ — is a density of heated water; V_1 is a volume of heated water (the volume of the shadow) with taking into account subtraction of the volume of a part of the end of the optical fiber's end immersed in the warmed-up liquid; D_2 is a diameter of the vapor bubble; D_1 is a diameter of heated water (shadow). Since the shape of the bubble and the shadow is a non-ideal flattened sphere, the present study uses an equivalent diameter calculated by the formula $D = \sqrt[3]{D_h^2}\sqrt[3]{D_g}$, where D_h is a transverse diameter, D_g is a longitudinal diameter (that is coaxial to the optical fiber). Substituting the values of D_1 and D_2 from Fig. 3 provides: $m_2/m_1 = 0.04 \pm 0.01$. It means that approximately 4 % of heated water boils up (transits into vapor). We note that it is an upper estimate, which assumes that the entire bubble is filled with vapor when its sizes are the highest. In reality, the bubble gets a considerable part of its volume by inertia of the liquid moving behind a bubble boundary. The liquid stretches the bubble due to inertia, thereby providing it with an additional volume. Therefore, the true mass portion of boiled-up water will be even lower than the given estimate.

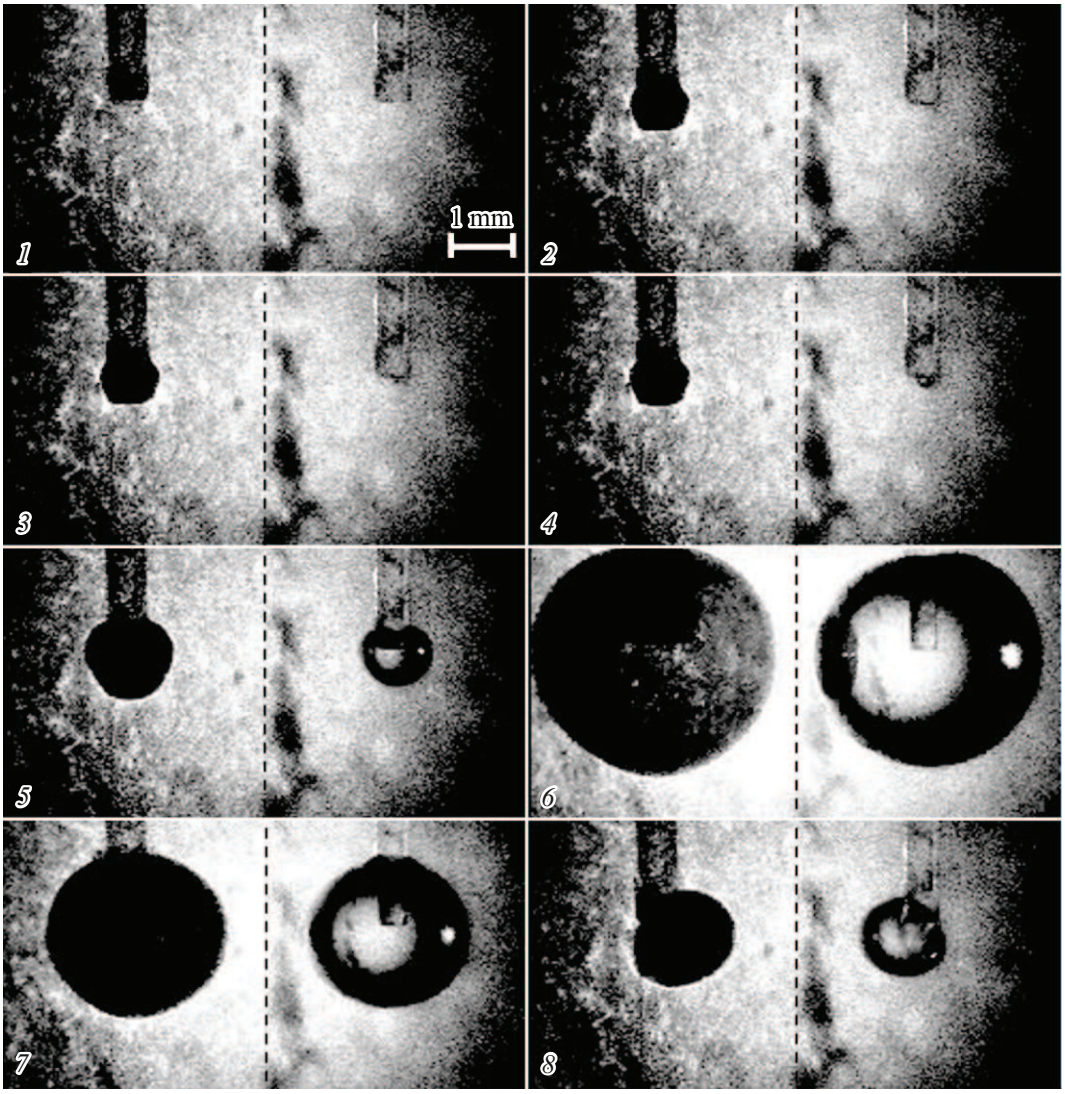

Figure 3. Same-moment image of the vapor bubble (to the left of the dashed line) and its shadow (to the left of the dashed line) as well as the area of water heating under effect of laser radiation, which is obtained according to the diagram of Fig. 1, *b*. The video-recording rate is 252 000 fps. The time between the frames *1*, *2*: $\Delta t_{12} = 68.47$ ms; between the frames *2*, *3*: $\Delta t_{23} = 5\,\mu$s; between the frames *3*, *4*: $\Delta t_{34} = 5\,\mu$s; between the frames *4*, *5*: $\Delta t_{45} = 35\,\mu$s; between the frames *5*, *6*: $\Delta t_{56} = 340\,\mu$s; between the frames *6*, *7*: $\Delta t_{67} = 234\,\mu$s; between the frames *7*, *8*: $\Delta t_{78} = 50\,\mu$s.

2. Model of heating water with continuous laser radiation

A system of equations, which models water heating, includes a continuity equation (1), a momentum conservation equation (2) and an energy conservation equation (3):

$$\frac{\partial \rho_l \mathbf{v}}{\partial t} + \nabla \cdot (\mathbf{v}\rho_l) = 0, \tag{1}$$

$$\frac{\partial \rho_l \mathbf{v}}{\partial t} + \nabla \cdot (\rho_l \mathbf{v}\,\mathbf{v}) = -\nabla p + \nabla[\mu_l(\nabla \mathbf{v} + \nabla \mathbf{v}^T)], \tag{2}$$

$$c_{pl}\frac{\partial \rho_l T}{\partial t} + \nabla \cdot (\mathbf{v}\rho_l c_p T) = \nabla(\lambda_l \nabla T) + Q. \tag{3}$$

Here, $\mathbf{v}$ is a velocity; T is the temperature; p is pressure; ρ_l, μ_l, c_{pl}, λ_l are density, viscosity, heat capacity, thermal conductivity of water, respectively. A source in the equation (3) Q describes distribution of the density of the flow of laser radiation flow with taking into account its absorption in water by the Bouguer-Lambert-Beer law [15]:

$$Q = kQ_0 \exp(-kz). \tag{4}$$

Here, Q_0 is the laser radiation flow density at the end face of the optical fiber, z is a distance from the end face of the optical fiber parallel to its axis to a point of the medium, k is an absorption coefficient. Impact by the source (4) is limited by a cylindrical area that is adjacent to the end face of the optical fiber (Fig. 5). This limitation is related to propagation of laser radiation along the optical fiber axis and with weak angular scattering in relation to the axis, outside of this area the function Q is zero. The experiments use laser radiation with the wavelength of 1.47 μm, for which the coefficient $k = 2850\,\mathrm{m}^{-1}$ [16]. $Q_0 = 4P/(\pi D^2) = 1.77 \cdot 10^7\,\mathrm{W/m}^2$,

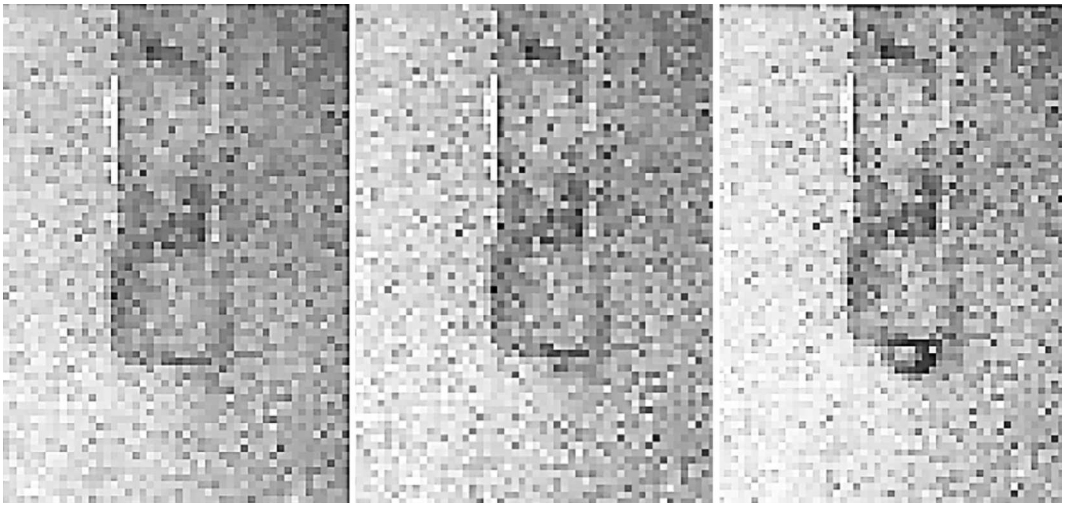

Figure 4. Frames of appearance of the vapor bubble on the end face of the optical fiber immersed in water. The time between three consecutive frames is 5 μs. The video-recording rate is 252 000 fps.

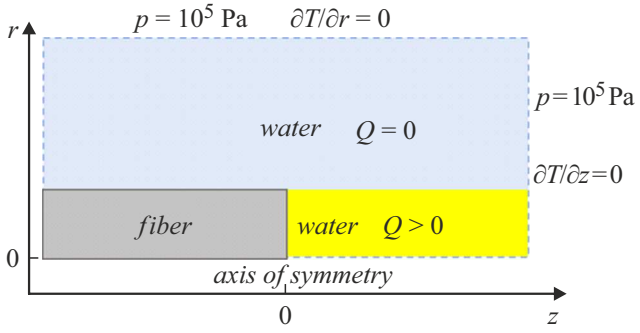

Figure 5. Computational domain with the sizes 0.005×0.01 m. A size of the square element of the mesh is 5 μm. The length of the optical fiber is 0.001 m.

where $P = 5$ W is power of laser radiation, $D = 600\,\mu$m is the diameter of the fiber. The equation (3) does not include a dissipation source, since influence of viscous heating can be neglected in the considered process of laser heating.

The density and viscosity of water depend on the temperature [17] (under atmospheric pressure). Heat capacity and thermal conductivity are considered to be constant. Distribution of the temperature in the optical fiber is determined from the thermal conductivity equation:

$$\rho_q c_{pq} \frac{\partial T_q}{\partial t} = \nabla(\lambda_q \nabla T_q), \tag{5}$$

where the index q means that physical characteristics belong to the material of the optical fiber (quartz).

The problem is solved in an axisymmetric formulation in the cylindrical system of coordinates (r, z). The computational domain is a rectangle that consists of two zones — the optical fiber and its surrounding two-phase medium water-vapor (Fig. 5). The walls and the end face of the optical fiber are provided with a no-slip condition: $\mathbf{v} = 0$. A condition of ideal thermal contact (equality of the temperatures and the thermal flows) and the no-slip condition is specified on surfaces of contact of the solid phase and the liquid phase. Atmospheric pressure and the zero thermal flow are specified at external boundaries of the computational domain that contains the liquid medium. At the initial moment of time, the entire computational domain has the zero velocity, atmospheric pressure $p = 10^5$ Pa and the initial temperature $T_0 = 16\,^\circ$C specified.

The system (1)–(5) is solved in a physical modeling environment ANSYS FLUENT 2021 on a uniform square mesh with the element size $d = 5\,\mu$m within the framework of a finite volume method. An iteration procedure of calculation of pressure and the velocity is implemented within the SIMPLE algorithm [18] for an incompressible fluid.

3. Model of vapor formation–condensation

The two-phase medium „water–vapor“ is considered. A law of variation of each of the phases is written as

$$\frac{\partial \alpha_g \rho_g}{\partial t} + \nabla(\alpha_g \rho_g \mathbf{v}) = \dot{m}_g,$$

$$\frac{\partial \alpha_l \rho_l}{\partial t} + \nabla(\alpha_l \rho_l \mathbf{v}) = \dot{m}_l, \tag{6}$$

where $\mathbf{v}$ is the velocity of the two-phase medium; α_g, α_l is a volume fraction of vapor and water, respectively; $\alpha_g + \alpha_l = 1$. The indices g and l designate that the characteristics belong to the vapor phase and the liquid phase, respectively; $\dot{m}_g/\dot{m}_l$ — a mass exchange source. A mechanism of interphase mass exchange is represented by the model of evaporation-condensation [19], in which a rate of vapor formation and condensation is proportional

to a difference between the current temperature and the saturation temperature:

$$\dot{m}_g = -\dot{m}_l = \gamma_g \alpha_l \rho_l \sqrt{\frac{T_{sat}(P_0)}{T_{sat}(P)}} \left(\frac{T - T_{sat}(P)}{T_{sat}(P)} \right),$$

$$\text{if } T > T_{sat}, \quad \alpha_g > \varepsilon_g, \tag{7}$$

$$\dot{m}_l = -\dot{m}_g = \gamma_l \alpha_g \rho_g \sqrt{\frac{T_{sat}(P_0)}{T_{sat}(P)}} \left(\frac{T_{sat}(P) - T}{T_{sat}(P)} \right),$$

$$\text{if} T < T_{sat}, \quad \alpha_l > \varepsilon_l, \tag{8}$$

where γ_g/γ_l are coefficients of vapor formation/condensation; $\varepsilon_g, \varepsilon_l$ — is a minimum fraction of the phase, at which mass exchange takes place; $T_{sat}(P)$ is the saturation temperature. We assume that the mass exchange coefficients γ_g, γ_l are constant magnitudes. The saturation temperature depends on pressure by a formula that is an approximation of the experimental data for water [17]:

$$T_{sat} = 268.283\,\text{K} + 0.04946\,\text{K} \cdot \left(\ln\left(\frac{P}{1Pa} \right) \right)^{3.13115}.$$

The equations (5)–(7) are supplemented with equations of momentum change and heat influx in the two-phase medium:

$$\frac{\partial \rho \mathbf{v}}{\partial t} + \nabla \cdot (\rho \mathbf{v}\,\mathbf{v}) = -\nabla p + \nabla[\mu(\nabla \mathbf{v} + \nabla \mathbf{v}^T)] + \mathbf{F}, \tag{9}$$

$$\frac{\partial c_p \rho T}{\partial t} + \nabla \cdot (\mathbf{v} \rho c_p T) = \nabla(\lambda \nabla T) + L \cdot \dot{m}_l + W. \tag{10}$$

where W is a heating source caused by viscous friction; L is latent heat of vapor formation (condensation); $\mathbf{F}$ is a volume force acting at a phase interface and modeling surface tension; c_p, ρ, λ, μ — heat capacity, density, thermal conductivity and viscosity of the two-phase medium, respectively. The heat influx equation (10) omits a laser heating source, since the mass exchange process takes place significantly faster than a process of warm-up to the saturation temperature (approximately in 50 times). Therefore, influence by the source (4) can be neglected when modeling dynamics of the vapor bubble.

The characteristics of the medium „water-vapor“ are written as

$$\rho = \alpha_g \rho_g + \alpha_l \rho_l, \quad \lambda = \alpha_g \lambda_g + \alpha_l \lambda_l,$$

$$\mu = \alpha_g \mu_g + \alpha_l \mu_l, \quad c_p = \alpha_g c_{pg} + \alpha_l c_{pl}. \tag{11}$$

The characteristics of the liquid phase corresponds to those previously described for the system (1)–(3). The density of the vapor phase is specified by means of an equation of state of the ideal gas $\rho_g = pM/(RT)$, where M is a molar weight of vapor, R is the universal gas constant. This representation (10) corresponds to a known method of „Volume of Fluid“ [5]. An expression for the volume force $\mathbf{F}$ is written as [20]:

$$\mathbf{F} = \frac{2\sigma\rho\kappa\nabla\alpha_g}{(\rho_g + \rho_l)}, \tag{12}$$

where $\sigma = (0.073\,\text{N} \cdot m^{-1}) \cdot (600\,\text{K} - T)$ is a coefficient of surface tension, which linearly depends on the temperature [17]; κ — curvature of the interphase boundary. Thermal conductivity λ_g, heat capacity c_{pg} and viscosity μ_g of the vapor phase are constant. The equation (9) omits a term that characterizes natural convection in the gravitational force field, since the cavitation process is much faster than a process of surfacing of the vapor bubble.

The system (5)–(10) as well as the system (1)–(5) is solved in the physical modeling environment ANSYS FLUENT 2021. Optimal selection of the mesh size $d = 5\,\mu$m when using the method of „Volume of Fluid“ was previously investigated in the study [5]. Dynamics of the two-phase medium is calculated by applying the SIMPLE algorithm for the incompressible fluid.

The equations with the mass exchange sources (7), (8) are additionally supplemented with limitations for the minimum phase fraction, at which these sources operate. Since at the initial moment of time we specify an area that include only the liquid phase ($\alpha_l = 1$, $\alpha_g = 0$) and an area that contains the vapor phase ($\alpha_l = 0$, $\alpha_g = 1$), i.e. the vapor bubble, then mass exchange is possible only around the interface of the two phases. Consequently, modeling excludes the process of volume boil-up of the liquid phase in areas with superheated water ($T > T_{sat}$) and a process of volume condensation inside the bubble when $T < T_{sat}$ (T_{sat} is the saturation temperature). Thus, the considered model still retains correctness of physical interpretation of a numerical method that consists of modeling of surface mass exchange. Estimation of the coefficients of vapor formation and condensation is determined based on an experimentally observed velocity of motion of the bubble surface at the stage of growth and collapse. The study [21] has reviewed ranges of values of the mass exchange coefficients, which are used in studies of various authors and vary from 0.1 to $10^7\,\text{s}^{-1}$ depending on heating conditions, the mesh size and a shape of the interphase boundary. The following values are used in the presented study: $\gamma_g = 10^6\,\text{s}^{-1}$, $\gamma_l = 10^7\,\text{s}^{-1}$.

4. Results of modeling of laser heating of water

Numerically solving the system (1)–(5) makes it possible to find distribution of the temperature field depending on selection of power of laser radiation and the time of its effect. Fig. 6 shows the results of the experiment and computational modeling of the temperature during laser heating.

Fig. 6, *a* shows the shadow cast by warmed-up water during „at lumen“ shooting. The shadow appears due to variation of the water density during heating. Contours

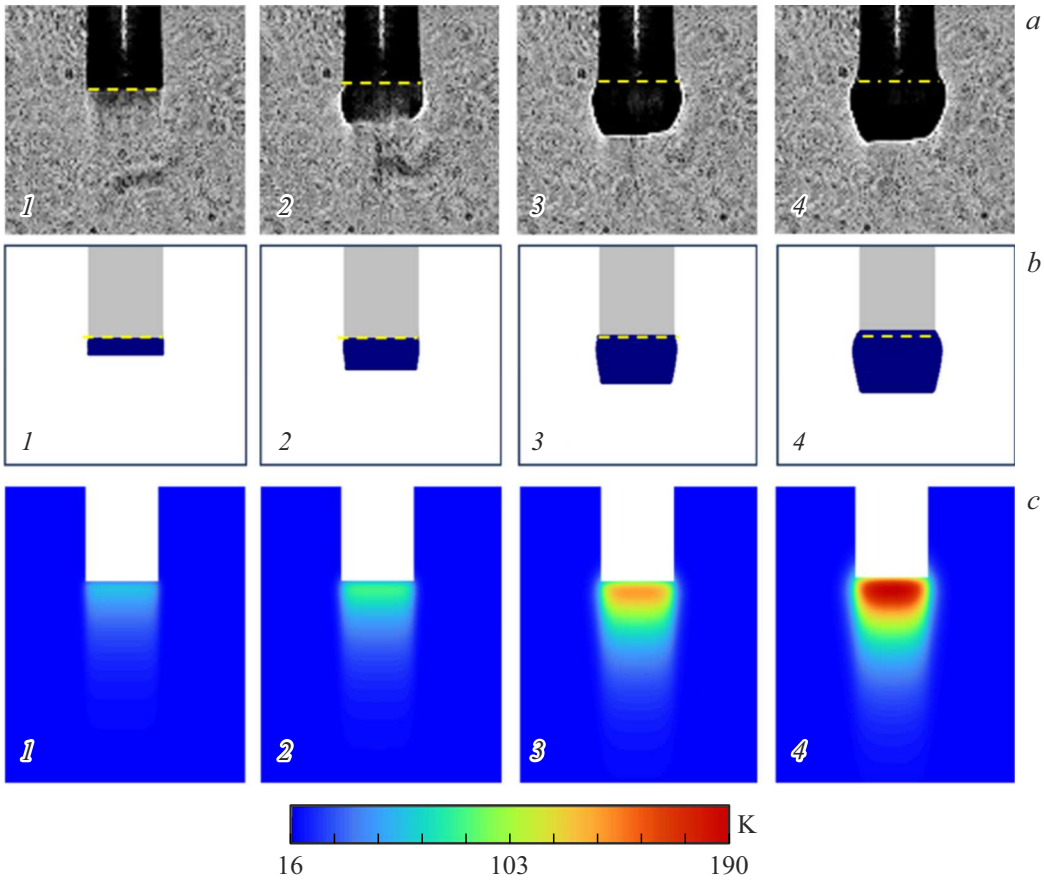

Figure 6. Heating of water near the end face of the optical fiber. *a* — the photo of the shadow formed during laser heating; *b* — the area, in which the calculated values of a temperature gradient modulus exceed $5 \cdot 10^5$ K/m; *c* — the calculated temperature field. The numbers of the frames correspond to the time $t_1 = 10$ ms, $t_2 = 15$ ms, $t_3 = 30$ ms, $t_4 = 45$ ms; $Q_0 = 1.77 \cdot 10^7$ W/m^2. The dashed line marks the surface of the end face of the optical fiber.

of the dark area being formed determine a boundary of the density gradient, at which a refractive ray of the light source stops hitting the camera lens. Fig. 6, *b* shows an area around the optical fiber, in which the values of the temperature gradient, which are calculated at the various moments of time, exceed $5 \cdot 10^5$ K/m. Fig. 6, *c* shows the calculated temperature field. The temperature modeling time $t = 45$ ms corresponds to the time of effect of the laser source in the experiment, which is followed by observation of a phenomenon of cavitation.

It is known that during surface boiling the bubbles start growing from microscopic air nuclei, which are initially distributed on irregularities of the solid phase surface as well as formed when inserting the optical fiber from the atmosphere into water. It was experimentally demonstrated that the first vapor bubble is nucleated on the surface in the center of the end face of the optical fiber, where an interface of the solid phase and the liquid phase is. Fig. 7 shows a distribution of the temperature (Fig. 6, *c*, the frame *4*) along the axis of symmetry of the optical fiber, which is calculated for the time of heating, at which cavitation is observed for the first time ($t = 45$ ms). It follows from Fig. 7 that the cavitation process starts when the surface of the end face of the optical fiber reaches the temperature exceeding the water saturation temperature, while the maximum of the temperature is at the distance of 0.12 mm to the end face. It has been demonstrated in the study [22] that this maximum of the temperature shifts in time. Water superheating near the end face results in the fact that the vapor bubble formed

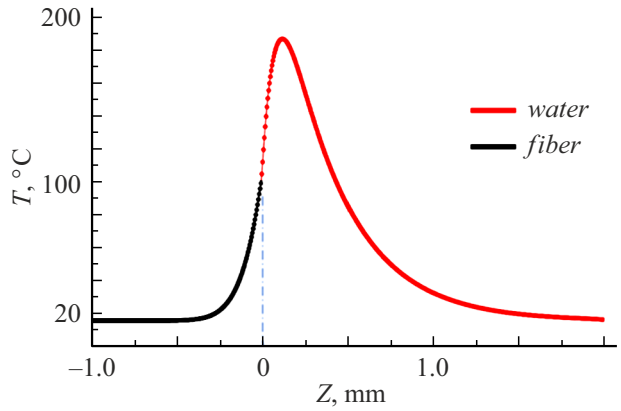

Figure 7. Distribution of the temperature along the axis of symmetry prior to the start of the vapor formation process.

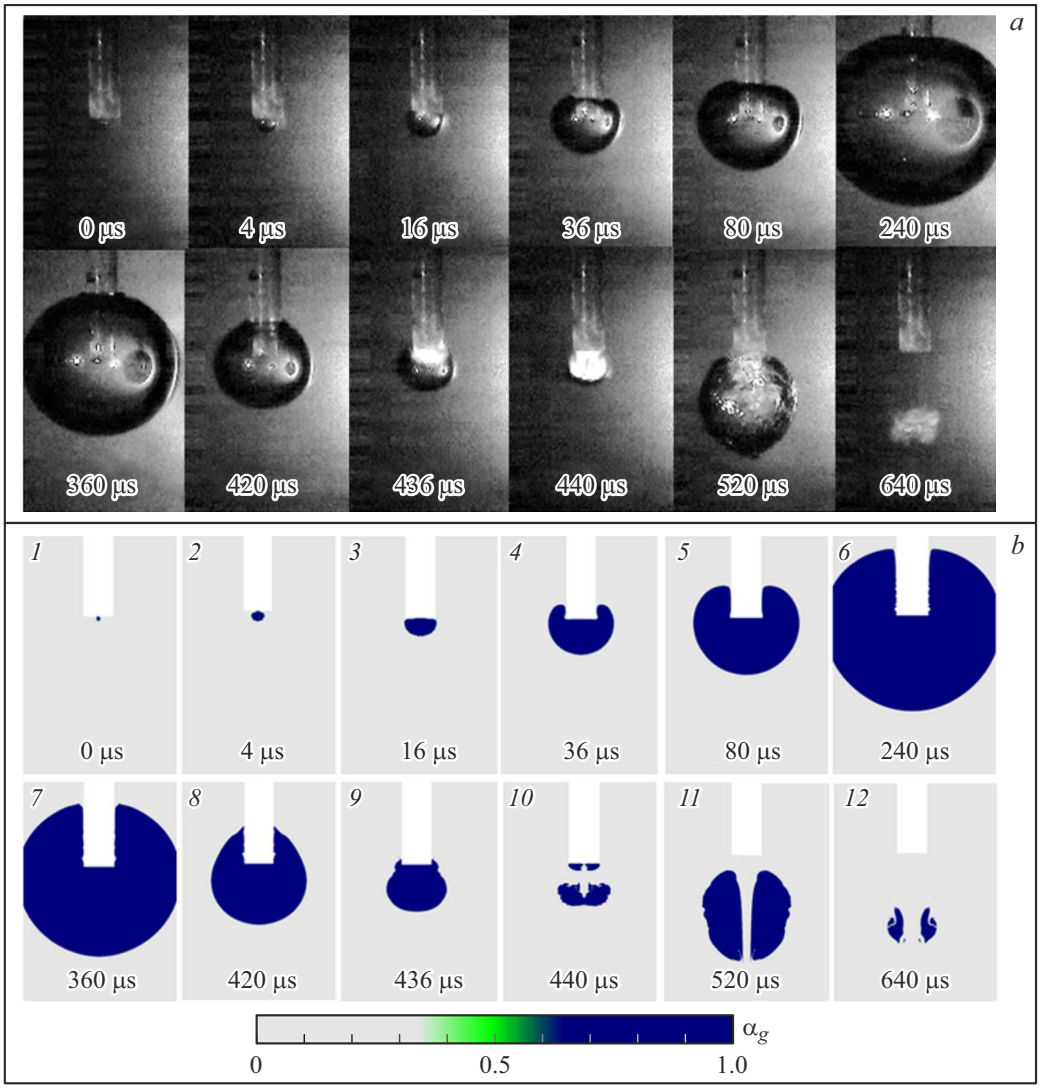

Figure 8. Variation of the size of the cavitation bubble in time: *a* — the result of experimental shooting, *b* — the numerical calculation. The fragments *1*–*6* correspond to the growth stage, while the fragments *7*–*10* correspond to the collapse stage.

on the surface of the end face starts acceleratedly growing due to intense vapor formation in the superheated area.

5. Results of modeling of the process of growth–collapse of the vapor bubble

Let us assume that at a certain new moment of time $t = 0$ the center of the end-face surface of the optical fiber has a bubble of the radius of $r_0 = 50\,\mu$m and internal pressure $p_0 = 1$ atm. The initial distribution of the temperature (Fig. 6, *c*, the frame *4*) and the velocity are specified as numerical solutions of the system of equations (1)–(5). A part of the surface of the bubble touches the area of the temperatures exceeding 100 °C. Thus, when $t > 0$ the process of vapor formation (7) is specified. The bubble grows when vapor pressure overcomes the surface tension force. Fig. 8 shows a bubble evolution process that is experimentally observed (Fig. 8, *a*) and resulted from computational modeling (Fig. 8, *b*) for the various moments of time.

Fig. 8 demonstrates good agreement of the numerical solutions and the experimental data. Fig. 8 (*6*) shows the maximum size of the bubble, so does the Fig. 8 (*10*) the minimum size of the bubble, which it obtains as a result of collapse. At this moment, a warmed-up cumulative jet starts forming and it secondarily boils up in the next frame (Fig. 8 (*11*)). Secondary boiling-up occurs due to reduction of pressure in the moving heated liquid [14]. It is accompanied by formation of a typical tapered shape of a set of the bubble that result from the boiling-up moving liquid (a „projectile“). The secondary bubble is a torus, whose axis is taken by the warmed-up jet to move thereon. Further on, this torus also collapses to form the submerged jet (Fig. 8 (*12*)).

Fig. 9 shows the distribution of the temperature and the velocity of motion of the vapor phase as well as the

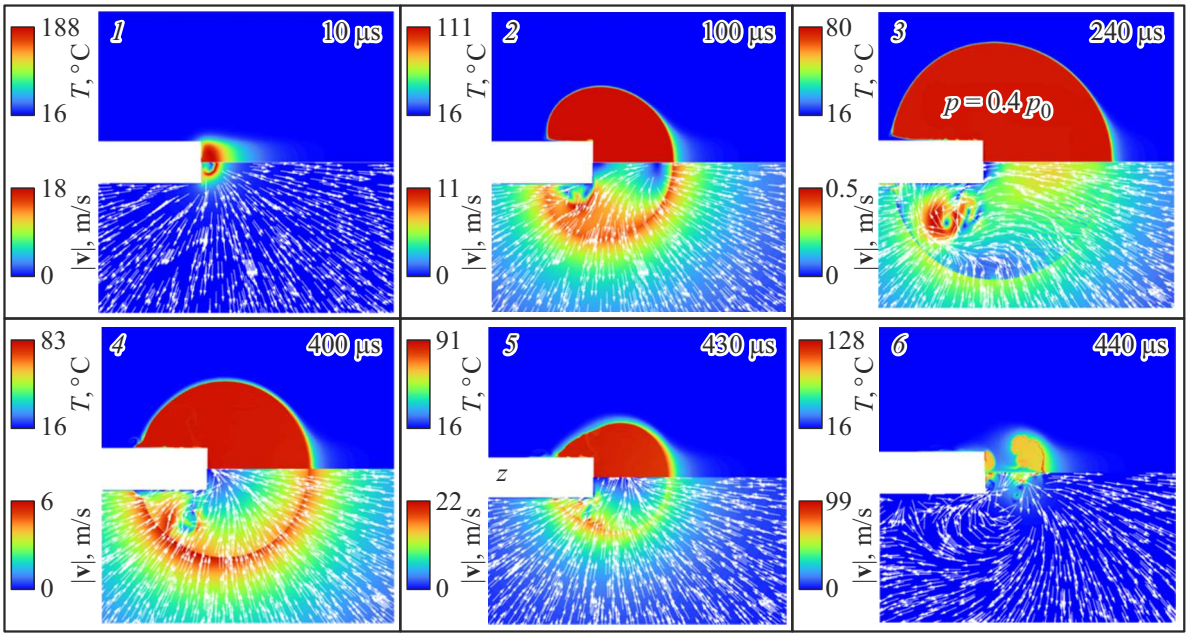

Figure 9. Temperature and the velocity of the two-phase medium during growth/collapse of the bubble.

liquid phase both in the bubble and the environment during cavitation at the various moments of time. It follows from Fig. 9 (*3*) that by the moment of start of collapse the temperature in the bubble reaches the values $\sim 80\,^{\circ}$C, which is below the saturation temperature, whereas pressure in the bubble drops to 0.4 atm. It is explained by inertial expansion of the bubble due to inertial motion of the liquid around the bubble. Inertial motion is imparted to the liquid by transfer of momentum from the bubble at the initial stage of its growth. After reaching the maximum size, the bubble starts acceleratedly collapsing. During collapse of the bubble, the vapor temperature increases (Fig. 9 (*4*–*6*)). It follows from the calculations that at the moment of collapse of the bubble and subsequent rebound (Fig. 9 (*6*)) the liquid phase obtains the maximum velocity ~ 100 m/s.

Further on, the process goes on as per Fig. 10, which shows origination and development of the cumulative jet.

According to the data of Fig. 10, the axis of symmetry has the cumulative jet formed and water motion is shaped as a toroidal vortex. The first such vortex takes place when water moving at the velocity ~ 30 m/s punches the bubble surface (Fig. 10 (*1*, *2*)). At this time, as a result of secondary boiling-up the area with vapor expands around the end face of the optical fiber. Further on, in Fig. 10 (*3*) collapse of the secondary vapor phase results in formation of the second cumulative jet that creates another toroidal vortex (Fig. 10 (*4*)), in which the liquid moves. Later on, vapor residuals condense and the submerged jet is formed. Fig. 10 (*5*, *6*) shows motion of water without the vapor phase.

The temperature of the cumulative jet reaches the maximum value $T = 60\,^{\circ}$C at the distance of 5 mm to the end face of the optical fiber, where its velocity is approximately equal to ~ 10 m/s. It should be noted that thermocavitation can be accompanied by more than 3–5 cycles of growth-collapse of the bubble, during which toroidal structures („rings“) are formed.The „rings“ prevent heat exchange with the environment, thereby making it possible to preserve heat of the liquid contained therein at the large distances. Thermocavitation depends on power of laser radiation, presence of uncondensed gases in the liquid and the initial temperature of water.

Conclusion

The results of the experimental study demonstrate that under effect of continuous laser radiation the vapor bubble originated on the surface of the end face of the optical fiber, and it first grows and then acceleratedly collapses. At the same time, less than 4 % of heated water is converted into vapor. The bubble growth results in formation of a time-varying layer of warmed-up, but unboiled-up water on its surface. The calculations demonstrate that the average temperature of this layer during bubble collapse varies within the range from $80\,^{\circ}$C to $60\,^{\circ}$C and determines the temperature of the cavitation jet. It is found that the cavitation jet has the toroidal vortices formed and they contribute to heat transfer over long distances through the cold liquid medium. The obtained estimate of the temperature is of high practical significance and defines the possibility of using continuous laser radiation in the liquid medium as a promising method of local surgery and in other medicine fields as well as for sanitizing technical surfaces.

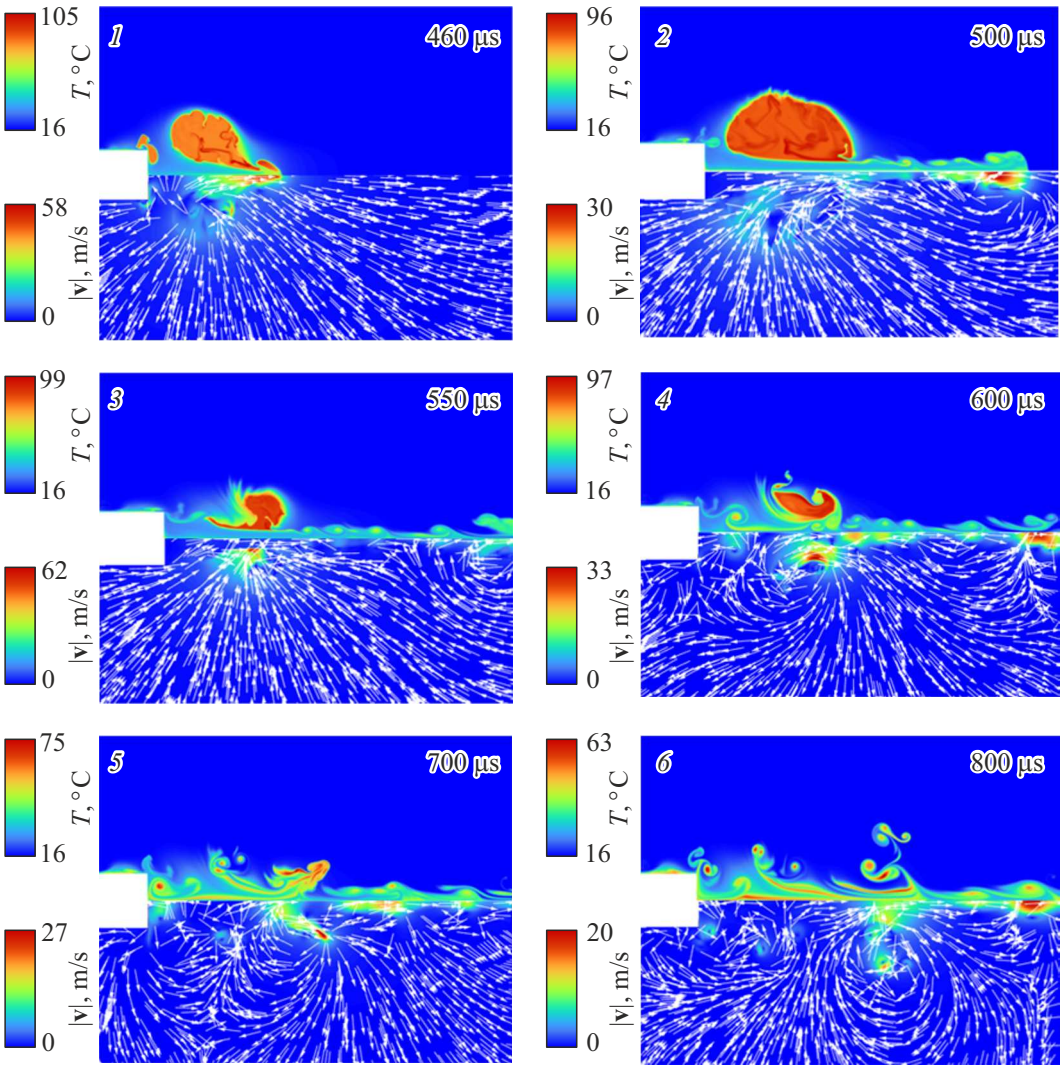

Figure 10. Velocity and the temperature of the cumulative jet at the various moments of time.

Funding

This study was financially supported by the Russian Science Foundation No. 22-19-00189-P.

Conflict of interest

The authors declare that they have no conflict of interest.

References

[1] S.A. Zhukov, S.Yu. Afanas'ev, S.B. Echmaev. Intern. J. Heat Mass Transfer, **46**, 3411 (2003).
[2] V.M. Chudnovskii, A.A. Levin, V.I. Yusupov, M.A. Guzev, A.A. Chernov. Intern. J. Heat and Mass Transfer, **150**, 119286 (2020). https://doi.org/10.1016/j.ijheatmasstransfer.2019.1192860017-9310
[3] M. Felix, A. Ellis. Appl. Phys. Lett., **1971** (19), 484 (1971).
[4] W. Lauterborn, H. Bolle. J. Fluid Mech., **1975** (72), 391 (1975). https://doi.org/10.1016/j.ijheatmasstransfer.2019.119286 0017-9310
[5] R.V. Fursenko, V.M. Chudnovskii, S.S. Minaev, J. Okajima. Intern. J. Heat and Mass Transfer, **163**, 120420 (2020). DOI: 10.1016/j.ijheatmasstransfer.2020.120420
[6] A.V. Kulik, S.N. Mokrin, A.M. Kraevskii, S.S. Minaev, M.A. Guzev, V.M. Chudnovskii. Tech. Phys. Lett., **48** (1), 60 (2022). DOI: 10.21883/TPL.2022.01.52472.18949
[7] M. Koch, J.M. Rosselló, C. Lechner, W. Lauterborn, R. Mettin. Fluids, **2022** (7), 2 (2022). DOI: 10.3390/fluids7010002
[8] E. Kadivar, T.-H. Phan, W.-G. Park, O. el Moctar. Phys. Fluids, **33**, 113315 (2021). https://doi.org/10.1063/5.0070847
[9] F. Reuter, C.-D. Ohl. Appl. Phys. Lett., **118**, 134103 (2021). DOI: 10.1063/5.0045705
[10] S. Gonzalez-Avila, F. Denner, C.-D. Ohl. Phys. Fluids, **33**, 032118 (2021). DOI: 10.1063/5.0043822
[11] V.A. Kosyakov, R.V. Fursenko, V.M. Chudnovskii, S.S. Minaev. Intern. Commun. Heat and Mass Transfer, **148**, 107053 (2023). https://doi.org/10.1016/j.icheatmasstransfer.2023.107053

[12] J.P. Padilla-Martinez, C. Berrospe-Rodriguez, G. Aguilar, J.C. Ramirez-San-Juan, R. Ramos-Garcia. Phys. Fluids, **26**, 12 (2014). https://doi.org/10.1063/1.4904718
[13] V.I. Yusupov. Russ. J. Phys. Chem., **13**, 1245 (2019). https://doi.org/10.1134/S1990793119070297
[14] A.A. Chernov, M.A. Guzev, A.A. Pil'nik, T.P. Adamova, A.A. Levin, V.M. Chudnovskii. Dokl. RAN. Fizika, tekhnicheskie nauki, **501**, 54 (2012) (in Russian). DOI: 10.31857/S2686740021060067
[15] T.G. Mayerhöfer, S. Pahlow, J. Popp. Chem. Phys. Chem., **21** (18), 2029 (2020). DOI: 10.1002/cphc.202000464
[16] R. Deng, Y. He, Y. Qin, Q. Chen, L. Chen. J. Remote Sensing, **16** (1), 192 (2012).
[17] Electronic source. Engineering ToolBox (2001) [online] Available at: https://www.engineeringtoolbox.com [Accessed 01.12.2024].
[18] S.V. Patankar. *Numerical Heat Transfer and Fluid Flow* (Hemisphere, Washington, DC, 1980)
[19] W.H. Lee. *Pressure iteration scheme for two-phase flow modeling* in Multiphase Transport Fundamentals, Reactor Safety, Applications, ed. by T. Veziroglu (Hemisphere Publishing, Washington, DC, 1980), p. 407–432.
[20] J.U. Brackbill, D.B. Kothe, C. Zemach. J. Comput. Phys., **100**, 335 (1992).
[21] Yu. Zhang, G. Li, G. Zhang, S. Ding. Appl. Thermal Eng., DOI: 10.1016/j.applthermaleng.2023.120872
[22] V.I. Yusupov, A.N. Konovalov. Intern. J. Thermal Sci., **203**, 109131 (2024). https://doi.org/10.1016/j.ijthermalsci.2024.109131

Translated by M.Shevelev